

Aalborg Universitet



**AALBORG
UNIVERSITY**

Comprehensive Comparison of Rotor Permanent Magnet and Stator Permanent Magnet Flux-Switching Machines

Su, P.; Hua, W.; Wu, Z.; Chen, Z.; Zhang, G.; Cheng, M.

Published in:
IEEE Transactions on Industrial Electronics

DOI (link to publication from Publisher):
[10.1109/TIE.2018.2875636](https://doi.org/10.1109/TIE.2018.2875636)

Publication date:
2019

Document Version
Accepted author manuscript, peer reviewed version

[Link to publication from Aalborg University](#)

Citation for published version (APA):
Su, P., Hua, W., Wu, Z., Chen, Z., Zhang, G., & Cheng, M. (2019). Comprehensive Comparison of Rotor Permanent Magnet and Stator Permanent Magnet Flux-Switching Machines. *IEEE Transactions on Industrial Electronics*, 66(8), 5862-5871. Article 8495026. <https://doi.org/10.1109/TIE.2018.2875636>

General rights

Copyright and moral rights for the publications made accessible in the public portal are retained by the authors and/or other copyright owners and it is a condition of accessing publications that users recognise and abide by the legal requirements associated with these rights.

- Users may download and print one copy of any publication from the public portal for the purpose of private study or research.
- You may not further distribute the material or use it for any profit-making activity or commercial gain
- You may freely distribute the URL identifying the publication in the public portal -

Take down policy

If you believe that this document breaches copyright please contact us at vbn@aub.aau.dk providing details, and we will remove access to the work immediately and investigate your claim.

Comprehensive Comparison of Rotor Permanent Magnet and Stator Permanent Magnet Flux-Switching Machines

Peng Su, *Student Member, IEEE*, Wei Hua, *Senior Member, IEEE*, Zhongze Wu, *Member, IEEE*, Zhe Chen, *Senior Member, IEEE*, Gan Zhang, *Member, IEEE*, Ming Cheng, *Fellow, IEEE*

Abstract—This paper compares two flux-switching machines, namely, one stator permanent-magnet flux-switching (SPM-FS) machine and one rotor permanent-magnet flux-switching (RPM-FS) machine, with the same overall dimensions, main material properties and current density. The characteristics comparison is conducted from two perspectives, i.e. electromagnetic torque production mechanisms and torque (power)-sizing equations. The harmonics contribution to average electromagnetic torque is analyzed based on the modulation principle and gearing effect, which reflects the similarities and differences between two FS machines in torque production mechanism. Moreover, torque performances are investigated from the viewpoints of magnetic parameters and electrical parameters. Then, electromagnetic performances including overload capability, flux-weakening capacity, and efficiency are analyzed and compared further. The predicted results indicate the RPM-FS machine exhibits larger torque capability, lower torque ripple, and improved flux-weakening capacity. The finite element analysis (FEA) predicted results are validated by experiments on two prototype machines.

Index Terms— Rotor permanent magnet, stator permanent magnet, flux switching, permanent magnet machine.

I. INTRODUCTION

IN recent years, stator-permanent magnet (PM) (SPM) flux-switching (SPM-FS) machines have attracted considerable attentions, due to the dramatic improvements of power (torque) density, efficiency and thermal dissipation ability, and are considered as a promising candidate for electric

Manuscript received Oct. 26, 2017; revised Mar. 5, 2018; accepted Sep. 24, 2018. This work was supported in part by the National Natural Science Foundation of China under Grant 51777032, Changjiang Scholars Program of China under Grant Q2017110. (Corresponding author: Wei Hua.)

Peng Su, Wei Hua, Gan Zhang and Ming Cheng are with the School of Electrical Engineering, Southeast University, Nanjing, 210096 China, (e-mail: supeng1639@126.com, huawei1978@seu.edu.cn, zhanggan@seu.edu.cn and mcheng@seu.edu.cn).

Zhongze Wu is with Department of Mechanical Engineering, University of Bath, Bath BA2 7AY, U.K. (e-mail: z.wu@bath.ac.uk).

Zhe Chen is with the Department of Energy Technology, Aalborg University, Aalborg 9220, Denmark (e-mail: zch@et.aau.dk).

vehicle (EV) and hybrid electric vehicle (HEV) applications [1]-[2]. However, due to the co-existence of PMs and armature windings in stator as shown in Fig. 1(a), the electrical loading of SPM-FS machines is significantly reduced, meanwhile, the magnetic saturation is serious in stator teeth with the reduced available space for both armature windings slots and stator iron laminations [3]. Then the torque capability is limited especially for the applications of EVs and HEVs, where normally a large armature current density is required due to the limited DC-link voltage supplied by batteries. To address the issues above, currently a novel rotor-permanent magnet flux-switching (RPM-FS) machine was proposed as shown in Fig. 1(b), which inherits the “flux-switching” principle of SPM-FS machines. The torque density can be enhanced further by removing the magnets from stator to rotor for the better usage of the rotor space and releasing the stator space to avoid serious iron saturation [4].

In preliminary design stage of electrical machines, the electromagnetic torque production mechanism and torque (power)-sizing equation are mostly important to investigate the operation principle and evaluate the torque capability, respectively. Recently, the torque production mechanism of flux-switching machines is investigated based on a novel perspective, namely magnetic field modulation principle [5]-[6], where it is found that the electromagnetic torque is not only contributed by the primitive harmonics of PM field and armature reaction field, but also produced by the corresponding modulated harmonic components [7]. The field modulation principle and gearing effect reveal the electromagnetic torque proportion of harmonic components, which is helpful to investigate the differences of flux-switching machines with novel topologies. On the other hand, the torque (power)-sizing equations are particularly important to promptly provide the relationship between key initial geometric dimensions and performance specifications [8]. Numerous research on the torque (power)-sizing equations of different machines are conducted, e.g. conventional interior-PM machines, vernier PM machines, double salient PM machines, axial-flux PM machines and out-rotor flux-switching PM machines, etc. [9]-[11]. In addition, the torque (power)-sizing equation also reflects the torque production mechanism, i.e. the interaction of magnetic loadings and electrical loadings.

In this paper, the electromagnetic torque characteristics of

flux-switching machines are investigated from two perspectives, namely, torque production mechanism and torque (power)-sizing equation. Meanwhile, a comparison of torque capability between two flux-switching machines with stator-PM and rotor-PM respectively is conducted in section II. Then, the electromagnetic performance of a pair of RPM- and SPM-FS machines are analyzed and compared further in section III, which reveals the merits and disadvantages of two machines comprehensively. The predicted results indicate the RPM-FS machine exhibits larger torque capability, lower torque ripple, and wider range of speed regulation. In section IV, the predicted results are verified by experiments on the two prototypes of RPM- and SPM-FS machines with the same stator outer diameter and stack length, followed by conclusions in section V.

II. TORQUE PRODUCTION MECHANISM AND TORQUE-SIZING EQUATION

The topologies of a pair of flux-switching machines with stator-PM and rotor-PM respectively are shown in Fig. 1, and key geometric dimensions and parameters are listed in Table I. For fair comparisons, the key geometric parameters, including stator outer diameter, stack length, air-gap, and rotor pole-pair number, are kept the same, and the material properties of magnets, stator and rotor irons are also identical. In addition, the effective armature current density of two flux-switching machines at the rated torque and the DC-link bus voltage are equal, i.e., $J_{a,rms}=5A/mm^2$ and $U_{dc}=600V$, respectively.

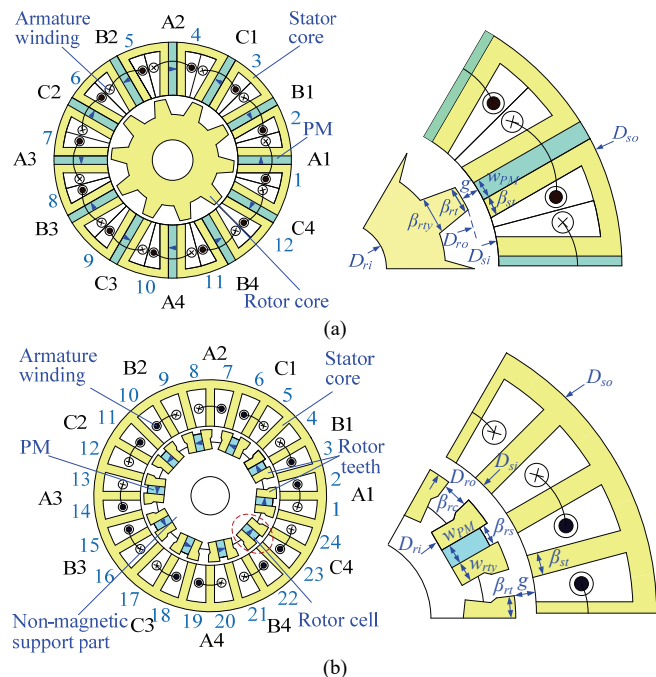


Fig. 1 The topologies of two flux-switching machines. (a) SPM-FS machine. (b) RPM-FS machine.

Based on the flux-switching operation principle, phase PM flux linkages and consequently, back-electro motive forces (back-EMFs) of both FS machines due to magnets solely are essentially sinusoidal [4]. Hence, the electromagnetic power P_e

of two machines can be expressed in a unified form as,

$$P_e = \frac{m}{T} \int_0^T e(t) \cdot i(t) dt = \frac{m}{2} E_{am} I_{am} \cos \theta \quad (1)$$

where, m is phase number, T is the period of phase back-EMF, E_{am} and I_{am} are the amplitudes of the fundamental phase back-EMF and armature current, respectively, and θ is the phase angle between phase back-EMF and armature current.

The amplitude of the fundamental phase back-EMF yields

$$E_{am} = N_{ph} \omega_r P_r \Phi_{PMm} \quad (2)$$

where, N_{ph} is winding turns per phase, ω_r is rotor speed, P_r is rotor pole-pair number, Φ_{PMm} is the fundamental amplitude of PM flux.

Since the d -axis inductance L_d is approximately equal to the q -axis inductance L_q in both RPM-FS and SPM-FS machines [4], the reluctance torque is negligible and $i_d=0$ control is suitable for both machines, i.e. $\theta=0^\circ$. Then, the electromagnetic torque can be expressed as:

$$T_e = \frac{P_e}{\omega_r} = \frac{m}{2} N_{ph} P_r \Phi_{PMm} I_{am} \quad (3)$$

It can be found that electromagnetic torque of RPM-FS and SPM-FS machines are significantly determined by the key magnetic parameter Φ_{PMm} and electrical parameter I_{am} .

TABLE I
KEY SPECIFICATIONS AND DIMENSIONS OF TWO FLUX-SWITCHING MACHINES

Specifications	RPM-FS	SPM-FS
Stator slots/Rotor pole-pair P_s/P_r	24/10	12/10
PM pole-pair P_{PM}	10	6
Based speed n_b (rpm)		1500
Stack length l_a (mm)		75
Stator outer diameter D_{so} (mm)		128
Stator inner diameter D_{si} (mm)	76.8	70.4
Air-gap length g (mm)		0.35
Rotor outer diameter D_{ro} (mm)	76.1	69.7
Rotor inner diameter D_{ri} (mm)	49.5	22
Stator teeth arc β_{st} (deg.)	7.2	7.5
Rotor teeth arc β_{rt} (deg.)	9.0	10.5
Rotor slot arc β_{rs} (deg.)	7.2	—
PM width w_{pm} (mm)	4.54	4.6
PM height h_{pm} (mm)	10.62	28.8
Iron lamination type		50WW470
PM type		N35SH
B_r (T) @20°C and 90°C		1.2/1.09
H_c (A/m) @20°C and 90°C		909456/833062
Number of turns per coil	66	70
Series coil number per phase		4
Wire diameter (mm)	0.85	0.95
Filling factor (%)		50
Winding factor	0.966	0.866

A. Analysis of Magnetic Parameters

The fundamental amplitude of phase PM flux Φ_{PMm} satisfies

$$\begin{aligned} \Phi_{PMm} &= 4B_{g \max} w_{rt} l_a k_{HC} k_{FL} k_d \\ &= \frac{2B_{g \max} \pi D_{so} k_{sio} c_s l_a k_{HC} k_{FL} k_d}{P_{PM}} \end{aligned} \quad (4)$$

where, w_{rt} is rotor-tooth-width, l_a is the effective stack length, k_{sio} is split ratio (the ratio of stator inner diameter D_{si} to stator outer diameter D_{so} for inner-rotor outer-stator machines), P_{PM} is PM pole-pair number, which is defined as the fundamental

harmonic order of the PM-MMF distribution. c_s is stator pole-arc coefficient, and B_{gmax} is the peak value of air-gap flux density, marked as B_{gmax} of A1 in Figs. 2(a) and 3(a), respectively. It should be emphasized that the general peak value (marked as “Peak value”) is ignored due to the localized saturation effect [12]. k_{HC} is the harmonic coefficient of phase flux to take harmonics influence into consideration, which is determined as the ratio of Φ_{PMm} to the peak value of phase flux. k_{FL} is the flux leakage coefficient, and k_d is the fundamental winding distribution factor. Since the parameters D_{so} , l_a , and P_{PM} are determined in the preliminary design process, Φ_{PMm} is dominantly influenced by the variables B_{gmax} , k_{sio} , and c_s in equation (4).

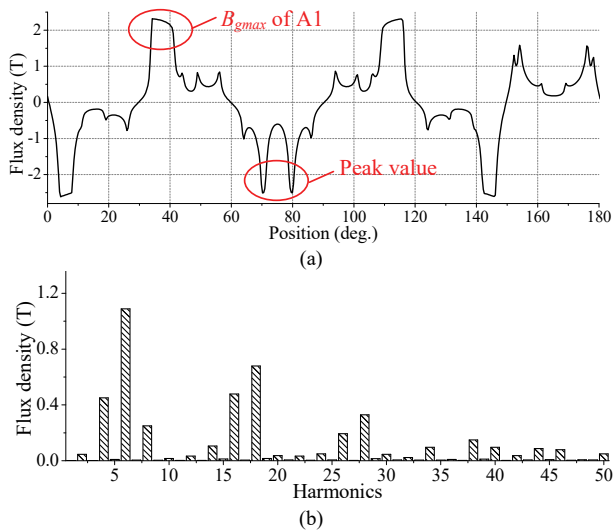


Fig. 2 The open-circuit air-gap flux density distribution of SPM-FS machine. (a) The air-gap flux density. (b) The harmonic distribution.

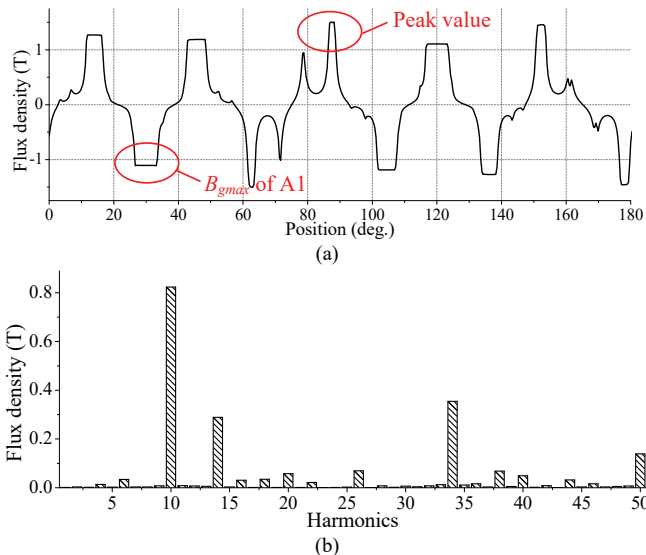


Fig. 3 The open-circuit air-gap flux density distribution of RPM-FS machine. (a) The air-gap flux density. (b) The harmonic distribution.

Based on the Fourier analysis, the flux-density harmonic distributions of two flux-switching machines are shown in Figs. 2(b) and 3(b). For the SPM-FS machine, the dominant harmonic components are 6th and 18th, produced by the

primitive PM-MMF (nP_{PM} , $n=1$ and 3), whereas the other harmonics with 4, 8, 16 and 28 pole-pairs ($|nP_{PM} \pm kP_r|$, ($n=1, k=1$, and $n=3, k=1$) are generated since the PM-MMF is modulated by the salient rotor teeth in air-gap field [7]. Similarly, for the RPM-FS machine, the dominant harmonics produced by the PM-MMF only are 10th and 50th components (nP_{PM} , $n=1$ and 5), meanwhile, if the modulation of salient stator teeth to rotor PM-MMF is taken into consideration, the harmonics of 14th and 34th components ($|nP_{PM} \pm kP_s|$, $n=1, k=1$) are generated [13]. It is worth noting that the primitive PM-MMF of RPM-FS machine contains the harmonics with 20 and 40 pole-pairs, i.e. nP_{PM} ($n=2$, and 4), which is different from the SPM-FS machine. Because the PMs in RPM-FS machines are magnetized with the same direction, and the rotor slot width β_{rs} is not equal to rotor cell gap β_{rc} as listed in Table I, which means that the even harmonic orders in PM-MMF cannot be cancelled, and then the corresponding harmonic components are produced in the air-gap flux density distribution as shown in Fig. 3(b).

Therefore, it can be concluded that the PM-MMF is modulated by the salient iron core, and the PM flux density distributions contain the harmonics produced by the PM-MMF (nP_{PM} , where $n=1, 2, \dots$), and the harmonics generated by the modulated PM-MMF ($|nP_{PM} \pm kP_r|$, $n, k=1, 2, \dots$), where the salient teeth number P_r is equal to P_r in SPM-FS machines and P_s in RPM-FS machines, respectively.

From the equation (4), the pole arc coefficient c_s is also a key parameter to influence Φ_{PMm} , which can be identified as:

$$c_s = \frac{B_{av}}{B_{gmax}} \approx \frac{\beta_{PMt}}{\pi / P_{PM}} = \frac{P_{PM} \beta_{PMt}}{\pi} \quad (5)$$

where B_{av} is the average flux density under one PM pole, and β_{PMt} is PM teeth arc as shown in Fig. 4.

It can be found that the PMs in RPM-FS machines is inserted between two adjacent rotor cores, and then, β_{PMt} is identical to rotor teeth arc β_r as shown in Fig.4. Since the PMs in RPM-FS machines are magnetized with the same direction, P_{PM} is 10, and then the corresponding pole arc coefficient c_s can be calculated to be 0.5. However, for SPM-FS machines, since the PMs are sandwiched by “C-type” stator cores, and magnetized in the opposite direction as shown in Fig. 1(a), P_{PM} is equal to 6. So, β_{PMt} is identical to the stator teeth arc, i.e. $\beta_{PMt} = \beta_{st}$, and consequently, $c_s = 0.25$ can be obtained.

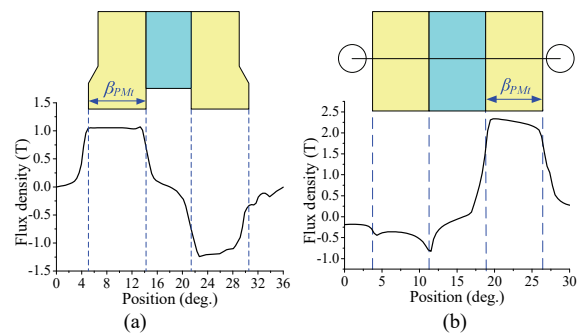


Fig. 4 The air-gap flux density distribution. (a) One PM pole-pair of RPM-FS machine. (b) Single PM pole of SPM-FS machine.

Obviously, the pole arc coefficient c_s of the RPM-FS

machine is higher than that of the SPM-FS one. In addition, the spilt ratio k_{sio} of RPM-FS machine is 0.6, which is slightly higher than that of the SPM-FS machine (0.55). Consequently, although the value of B_{gmax} in the SPM-FS machine (2.2T) is about 2 times of that of the RPM-FS machine (1.1T), the peak value of phase PM flux is slightly larger than that of RPM-FS machine as shown in Fig. 5. Furthermore, the PM flux of RPM-FS machine contains harmonics with odd pole-pair numbers, and the total harmonic distortion (THD) is higher (3.8%). Hence, the harmonic coefficient k_{HC} should be taken into consideration to precisely calculate Φ_{PMm} in equation (4).

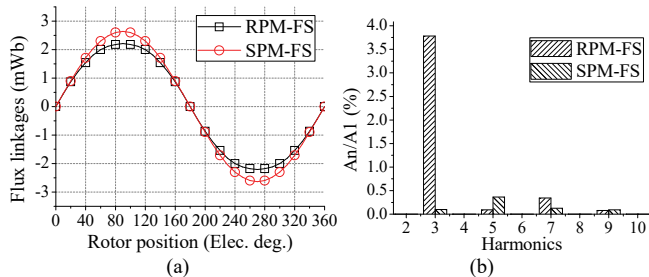


Fig. 5 The no-load PM flux linkages per turn. (a) PM flux linkage waveforms. (b) Harmonic distributions.

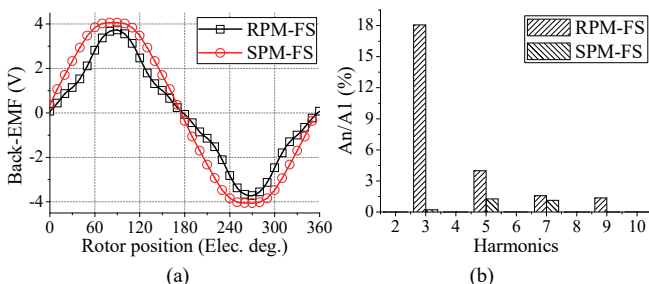


Fig. 6 No-load phase back-EMF per turn of two flux-switching machines @1500r/min. (a) Phase back-EMF waveforms. (b) Harmonic distributions.

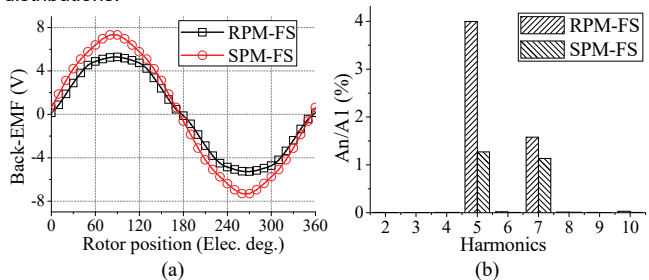


Fig. 7 No-load line back-EMF per turn of two flux-switching machines @1500r/min. (a) Line back-EMF waveforms. (b) Harmonic distributions.

Correspondingly, the open-circuit phase back-EMF waveforms per turn at the based speed of 1500r/min are shown in Fig. 6. By applying Fourier analysis, it can be found that the phase back-EMF waveform of the RPM-FS machine has the higher odd-order harmonics especially the 3rd-order component, which is agreed with the PM flux-linkage analysis. However, the 3rd-order harmonic can be cancelled by “Y”-connected armatures windings, and thus the line back-EMF waveform is more sinusoidal as shown in Fig. 7, where the fundamental amplitudes of the line back-EMF of the RPM-FS and SPM-FS machines is 5.4V and 7.19V, and the corresponding total

harmonic distortion (THD) is 4.36% and 1.70%, respectively.

B. Analysis of Electrical Parameters

The armature reaction MMF is produced by injecting 3-phase symmetrical and sinusoidal currents. The back-EMF vectors distributions of the slot conductors in two flux-switching machines are shown in Fig. 8. Based on the fundamental star vector theory [14], the armature winding pole-pair number P_a of the 24s/10p RPM-FS machine is equal to $P_{PM}=P_r=10$, and then it can be deduced that the armature reaction MMF contains the harmonics with $(2i-1)$ pole-pair multiplied by the greatest common divisor (GCD) of P_s and P_a , i.e. $4i-2$ ($i=1, 2, \dots$, but without triple multiples).

However, for the 12s/10p SPM-FS machine, the definition of P_a should be redefined, which is different from that of RPM-FS machine. Since the PMs are inserted between two adjacent stator cores and the slot number P_s is equal to $2P_{PM}$, it can be deduced that the $\text{GCD}(P_s, P_a)$ is P_s . If P_a is defined the same as that of the RPM-FS machine, namely, $P_a=P_{PM}$, then the corresponding spoke number N_{sp} of back-EMF vectors distributions in slot conductors can be obtained by $N_{sp}=P_s/\text{GCD}(P_s, P_a)$, which is identically equal to 2. Obviously, the result cannot match the combination condition of P_s and P_r , namely N_{sp} must be an integer multiplied by the phase number $m=3$ [13]-[14]. Therefore, for SPM-FS machines P_a is redefined as $P_a=|P_{PM}\pm P_r|$, and then the modulated PM-MMF harmonic components can be utilized to produce electromagnetic torque. The armature reaction harmonic orders of the 12s/10p SPM-FS machine are expressed as $4i$ ($i=1, 2, \dots$ without triple multiples).

In addition, since the rotor topologies of two flux-switching machines are both salient structures, the armature reaction MMF will be modulated by the rotor teeth. Then, the modulated harmonic orders of RPM-FS and SPM-FS machines can be identified as $|(4i-2)\pm jP_r|$ and $|4i\pm jP_r|$ ($j=0, 1, 2, \dots$), respectively, which can be verified by the results shown in Figs. 9(a) and (b).

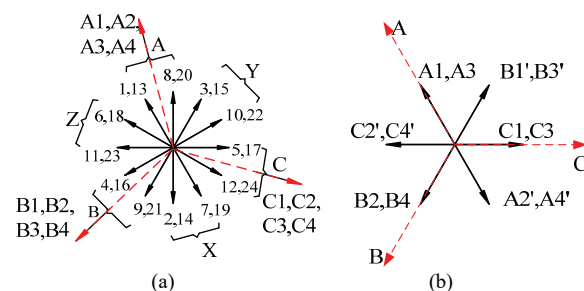


Fig. 8 The back-EMF distributions of slots conductors. (a) RPM-FS machine. (b) SPM-FS machine.

The amplitude of phase current I_{am} in equation (3) yields,

$$I_{am} = \frac{\sqrt{2}J_{a_rms}A_{slot}k_{sf}P_s}{8mN_{ph}} \quad (6)$$

where, A_{slot} is the armature slot area, and k_{sf} is the slot fill factor. Since the two machines are designed under air cooling condition, the rated phase current density is set to $J_{a_rms}=5\text{A/mm}^2$. Hence, I_{am} is mainly determined by the slot effective area $A_{slot}k_{sf}$ and the phase turns number N_{ph} . It should

be emphasized that N_{ph} can be cancelled further in torque-sizing equation, and then electromagnetic torque T_e is mainly influenced by $A_{slotk_{sf}}$ from the electrical loading perspective. Moreover, the value of $A_{slotk_{sf}}$ in the RPM-FS machine is 78.4mm^2 , which is 1.5 times of that of the SPM-FS one due to removed PMs from stator to rotor.

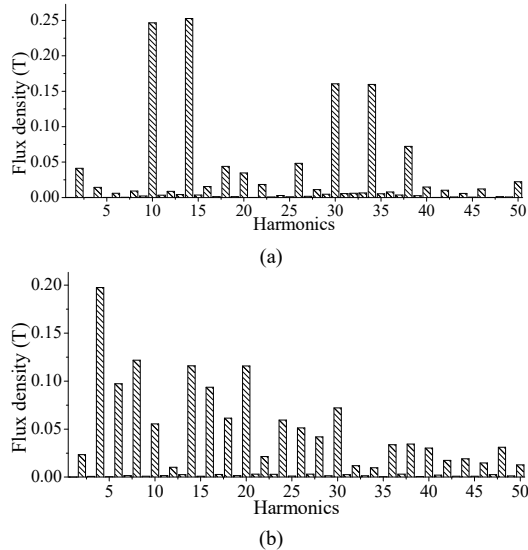


Fig. 9 Harmonic distributions of modulated armature reaction air-gap field. (a) RPM-FS machine, (b) SPM-FS machine.

C. Electromagnetic Torque Production

The electromagnetic torque is produced by the interaction between the harmonic components of magnetic loadings and electrical loadings as revealed by equation (7), which exhibit the same orders and rotating speeds [14].

$$T_e = -\frac{D_{sl}^2 l_a}{4} \int_0^{2\pi} B_g(\theta_r) A_{Wv}(\theta_r) d\theta_r \quad (7)$$

$$= \frac{\pi D_{sl}^2 l_a}{4} \sum_{v=1}^{\infty} B_{gv} A_{Wv} \cos\phi_v$$

where, B_{gv} is the harmonic component of magnetic loadings with v pole-pair, and A_{Wv} is the corresponding harmonic component of electrical loadings in armature windings with v pole-pair, and ϕ_v is the phase angle shift between B_{gv} and A_{Wv} . Based on the harmonic distributions of PM-MMF and armature reaction MMFs in Figs. 2, 3 and 9, the electromagnetic torque T_e contributions by air-gap field harmonics are shown in Fig. 10.

For the 24s/10p RPM-FS machine, the electromagnetic torque T_e is dominantly produced by the harmonics with 10 (83%), 14 (-11.5%) and 34 (21.4%) pole-pairs, which means the contribution of the harmonic with 10 pole-pairs is significantly higher than those of 14th and 34th harmonics, since the 10th harmonic is the fundamental component of PM-MMF from the magnetic loadings viewpoint, being higher than the modulated harmonics with 14 and 34 pole-pairs. Meanwhile, from the viewpoint of the armature reaction field, the dominant harmonic components contributing to T_e are also the primitive harmonics, i.e., $(4i-2)$ pole-pairs ($i=1, 2, \dots$, but without triple multiples).

For the 12s/10p SPM-FS machine, T_e is mainly attributed to 6 harmonic components, including 4th, 6th, 8th, 16th, 18th, and 28th. From the magnetic loadings perspective, the primitive harmonic components, namely 6th and 18th, produces 18% and 28.9% of the electromagnetic torque respectively, whereas the contributions by modulated harmonics with 4th, 8th, 16th and 28th is 28.5%, -14%, 29.2% and 9.5%, respectively. From the electrical loadings perspective, the primitive harmonics of armature reaction MMF ($4i$, where $i=1, 2, \dots$ without triple multiples) and the modulated harmonics ($|4i \pm jP_r|$, where $i=1, 2, \dots$ without triple multiples, $j=1, 2, \dots$) are both utilized to generate T_e . In general, the SPM-FS machine not only uses primitive harmonics in PMs and armature reaction fields, but also the modulated harmonics, which is different from that of RPM-FS machines.

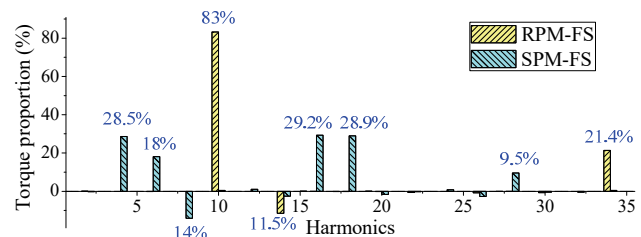


Fig. 10 Electromagnetic torque decompositions of the RPM-FS machine and SPM-FS machine.

TABLE II
THE KEY GEOMETRIC PARAMETERS OF TWO FLUX-SWITCHING MACHINES

Item	Geometric parameters	
	RPM-FS	SPM-FS
B_{gmax}	$\beta_{st}, \beta_{rt}, \beta_{rs}, WPM, k_{lrrt}, k_{sio}$	$\beta_{st}, \beta_{rt}, WPM, k_{sio}$
k_{sio}	k_{sio}	k_{sio}
c_s	β_{rt}	β_{st}
$A_{slotk_{sf}}$	β_{st}, k_{sio}	β_{st}, WPM, k_{sio}

On the other hand, based on the analysis of magnetic parameter Φ_{PMm} in equation (4) and electrical parameter I_{am} in equation (6), the electromagnetic torque equation can be evolved as equation (8), which can be utilized to estimate the electromagnetic torque directly.

$$T_e = \frac{\sqrt{2}\pi}{8P_{PM}} P_r P_s B_{gmax} D_{so} k_{sio} J_{a_rms} A_{slot} l_a c_s k_{HC} k_{sf} k_d k_{FL} \quad (8)$$

According to equation (8), the directly predicted electromagnetic torque T_e of the RPM-FS machine is 17.36Nm, and the error between the 2D-FEA estimation is 10.8%. For the SPM-FS machine, the directly obtained T_e is 16.9Nm, which is about 1.14 times of the 2D-FEA result. For both machines, the error between the analytical results and the 2D-FEA results can be attributed to the ignorance of magnetic saturation effect and the estimation of the flux leakage coefficient k_{FL} .

From equation (8), it can be seen that T_e is mainly influenced by the magnetic parameters B_{gmax} , k_{sio} and c_s in equation (4), and the electrical parameters $A_{slotk_{sf}}$ in equation (6). However, both the magnetic and electrical parameters are determined by the geometric dimensions shown in Table II. Hence, geometric parameters sensitivity are analyzed to explicitly reflect the influence of each design variable on the optimization objectives, i.e. electromagnetic torque and torque ripple.

D. Sensitivity Analysis of Geometric Parameters

Based on the derivation of torque-sizing equation (8), the key geometric parameters in flux-switching machines can be determined given the specification requirements. Meanwhile, the key geometric variables will impact on torque performances significantly, hence, the sensitivity analysis on electromagnetic torque T_e and torque ripple T_{ripple} are conducted based on the local sensitivity analysis (LSA) [15] and global sensitivity analysis (GSA) [16], and the result are shown in Table III.

TABLE III
SENSITIVITY ANALYSIS OF GEOMETRIC PARAMETERS OF TWO MACHINES

Topologies	Variables	Optimization objectives	
		T_e	T_{ripple}
RPM-FS machine	k_{sio}	0.33	1.44
	k_{hrt}	1.82	0.21
	β_{st}	0.49	0.44
	β_{rt}, β_{rs}	0.34	2.7
	w_{PM}, w_{rt}	0.21	0.04
SPM-FS machine	k_{sio}	0.462	4.3
	k_{hrt}	0.002	0.07
	β_{rt}	0.29	1.19
	β_{rty}	0.0198	0.153
	β_{st}, w_{PM}	0.717	2.31

From Table III some conclusions can be summarized:

(1) k_{sio} has dominant influence on T_e and T_{ripple} in both flux-switching machines, since it is not only the key variable in torque-sizing equation (8), but also it directly determines the magnetic loadings B_{gmax} and armature winding slot area $A_{slotk_{sf}}$ under a given stator outer diameter, which can further determine the torque capability.

(2) k_{hrt} exhibits the highest sensitivity on T_e in the RPM-FS machine due to the significant influence of PM volume and B_{gmax} . However, for the SPM-FS machine, k_{hrt} has little impact on T_e and T_{ripple} since the rotor structure is simple and robust, and k_{hrt} can change the magnetic saturation in rotor yoke only.

(3) From the topology of RPM-FS machines in Fig. 1(b), β_{rt} and β_{rs} are constrained by each other in the circumferential direction, and are analyzed comprehensively by GSA [16]. β_{rt} and β_{rs} are the key dimensions to determine c_s and B_{gmax} in torque-sizing equation, and consequently, T_e will be affected further. It is worth noting that β_{rt} and β_{rs} have the highest sensitivity on torque ripple, which indicates that T_{ripple} can be significantly reduced by optimizing the corresponding variables. Similarly, the sensitivity values of w_{PM} and w_{rt} are also calculated by GSA, which have little impacts on T_{ripple} . For the SPM-FS machine, the rotor structure is mainly determined by β_{rt} and β_{rty} , where β_{rt} has remarkable influences on T_e and T_{ripple} , and β_{rty} only has effect on T_{ripple} .

(4) From Figs. 1(a) and (b), the stator structure of SPM-FS machines is more complicated than that of RPM-FS machines, and the parameters β_{st} and w_{PM} are constrained by each other in the circumferential direction. The combined sensitivity analysis results are listed in Table III. It can be seen that β_{st} and w_{PM} have considerable influences on T_e and T_{ripple} , since they determine both magnetic and electrical loadings parameters in torque-sizing equation, i.e. B_{gmax} , c_s , and $A_{slotk_{sf}}$. However, for the RPM-FS machine, the stator structure parameter β_{st} only

has impact on $A_{slotk_{sf}}$, which affects T_e further.

III. ELECTROMAGNETIC PERFORMANCES COMPARISON

In this section, based on 2D-FEA, the electromagnetic performances of the RPM-FS machine and the SPM-FS machine are investigated and compared comprehensively.

A. Torque Performances

The rated electromagnetic torque versus rotor position waveforms of two flux-switching machines are shown in Fig. 11(a). It can be found that the average torque and torque ripple of the RPM-FS machine is 16.05Nm and 11%, respectively. However, the torque ripple without cogging torque is only 5%, hence, the predicted cogging torque waveform in Fig. 11(b) is the main reason for torque ripple and can be reduced by optimization further. For the SPM-FS machine, the average torque is 14.8Nm, which is 8% lower than that of the RPM-FS one. Meanwhile, the torque ripple of the SPM-FS machine is 22%, which is 2 times of that of the RPM-FS machine. However, the torque ripple without cogging torque can be dramatically reduced to 6% only as shown Fig. 11(a), since the peak-peak cogging torque of the SPM-FS machine is 3.4Nm, which is much higher than the RPM-FS machine as shown in Fig. 11(b).

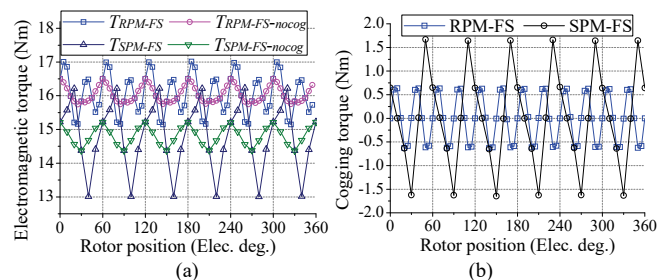


Fig. 11 Torque characteristics of two flux-switching machines. (a) Output torque. (b) Cogging torque.

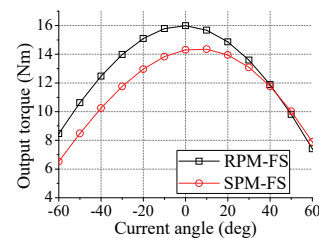


Fig. 12 Torque versus current angle.

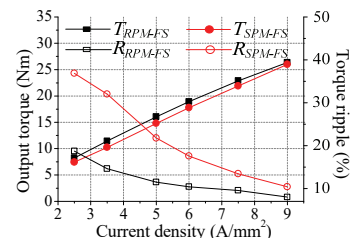


Fig. 13 Torque versus current density.

The output torques versus armature current angles (β) at the current density of $J_{a,rms}=5A/mm^2$ are shown in Fig. 12, where the RPM-FS and SPM-FS machines reach the maximum torque

when β is 0° and 5° , respectively, which means the dq -axes inductances L_d/L_q are approximately equal in both machines. Hence, the reluctance torques are negligible and $i_d=0$ control is suitable for both machines.

Fig. 13 shows the average torque versus current densities. It can be found that the output torque of RPM-FS machine is always larger than that of SPM-FS machine and the torque ripple ratio is smaller. Moreover, the output torque of RPM-FS machine increases linearly, as the armature current density rises, which is almost parallel to that of the SPM-FS machine. Hence, both of RPM-FS machine and SPM-FS machine have satisfactory overload capacity.

In addition, the consumed PM material mass (kg) and utilization ratio (torque per magnet mass) are listed in Table IV. It can be found that the PM utilization ratio of the RPM-FS machine is 59.4(Nm/kg), which is about 3.6 times of that SPM-FS machine. The core losses and PM losses are listed in Table IV, where the core losses are analyzed based on the improved Yamazaki's model [17, 18], and the PM eddy current losses are calculated by the 3D-FEA. The predicted efficiencies of two machines at rated operation point are almost same, being 90.2% and 90.9%, respectively.

B. Flux Weakening Capability

The constant-power speed range is another key characteristic of traction machines for EV and HEV applications. Generally, the flux-weakening ability of the PM brushless machines can be expressed by a flux-weakening coefficient k_{fw} [11]

$$k_{fw} = \frac{N_{ph} \Phi_{PMm}}{N_{ph} \Phi_{PMm} - L_d i_d} \quad (9)$$

where, L_d and i_d is the d -axis inductance and armature current, respectively. From Table IV, the flux-weakening capacities of two machines can be evaluated by equation (9). The coefficient k_{fw} of RPM-FS and SPM-FS machines is 2.47 and 1.51, respectively. Since both flux-switching machines can not realize completed flux-weakening, the maximum speed n_{max} can be evaluated as [19],

$$n_{max} = \frac{60}{2\pi P_r} \cdot \frac{U_{lim}}{N_{ph} \Phi_{PMm} - L_d i_d} \quad (10)$$

where U_{lim} is the limited voltage, which is determined by the DC-bus voltage. It can be found that the magnetic parameter $N_{ph} \Phi_{PMm}$, i.e., the d -axis PM flux linkage of the SPM-FS machine is larger than that of the RPM-FS one from Table IV, whereas the d -axis armature reaction flux-linkage $L_d i_d$, which is related to the electrical performance parameter I_{am} , is lower. Hence, the maximum speed of the RPM-FS machine can be obtained to be 4600r/min as shown in Fig. 14, which is about 1.8 times of that of the SPM-FS machine under the same DC-bus voltage. Meanwhile, the constant power range of the RPM-FS machine is also wider.

In addition, at the beginning of flux-weakening control, a higher i_d of the SPM-FS machine is utilized to offset the PM flux linkage due to the limited U_{dc} , which leads to a sharp reduction of i_q . Since the reluctance torque in both machines is negligible, the electromagnetic torque is approximately equal to the PM torque. Hence, T_e reduces significantly as shown in Fig. 14, and then, the peak power of the SPM-FS machine is lower

than that of the RPM-FS machine. In addition, the speed regulation range of RPM-FS machine can be improved further by adjusting the key geometric parameter k_{hrt} (the ratio of D_{ri} to D_{ro} as shown in Fig. 1(b)). In the case of $k_{hrt}=0.73$, $D_{ri}=55.6$ mm and $D_{ro}=76.1$ mm, the output torque of RPM-FS machine is reduced as 14.8Nm due to the lower PM volume utilization, which is the same as rated torque of SPM-FS machine. Then, k_{fw} is calculated as 2.75, and a larger maximum speed 5300r/min can be obtained.

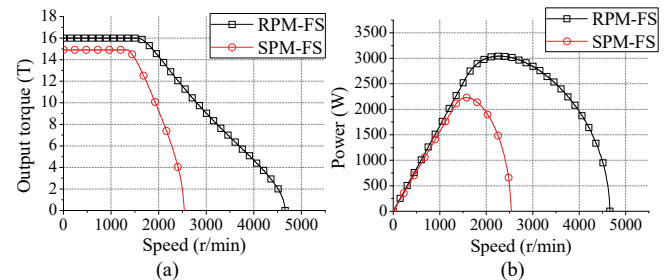


Fig. 14 Output torque and power with different speed of two flux-switching machines @ $J_{e,ms}=5$ A/mm² and $U_{dc}=600$ V. (a) The torque with versus speed. (b) The power versus speed.

TABLE IV
PERFORMANCE COMPARISON OF TWO FLUX-SWITCHING MACHINES

Specifications	RPM-FS	SPM-FS
Mass of stator iron (kg)	2.49	2.39
Mass of rotor and shaft (kg)	2.13	1.62
Mass of copper mass (kg)	2.0	1.24
Mass of PM (kg)	0.27	0.9
Total mass (kg)	6.89	6.15
R_{phase} (Ω) @25°C	1.2	1.9
PM flux linkage (Wb)	0.124	0.185
d -axis inductance L_d (mH)	8.80	11.64
q -axis inductance L_q (mH)	9.22	14.97
k_{fw}	2.47	1.51
Peak value of cogging (Nm)	1.4	3.4
Output torque (Nm)	16.05	14.8
Torque ripple (%)	11%	22%
$k_{T/PM}$ (Nm/kg)	59.4	16.4
Copper loss (W) @90°C	158.8	103.8
T_{out}/P_{cu} $k_{T/Pcu}$	0.101	0.142
Core loss (W)	59.74	51.47
PM loss (W)	3.92	30.95
Output power (W)	2520.9	2324.6
Efficiency (%)	90.2%	90.9%
Power factor	0.89	0.91

IV. EXPERIMENTAL VALIDATIONS

To validate the previous analysis and results, two prototypes of the RPM-FS and SPM-FS machines are manufactured, and experiments are carried out in this section. Figs. 15 and 16 show the two prototypes, and the main design dimensions are in accordance with those listed in Table I. It can be found that each PM of RPM-FS machine is fixed by the convex structure of the adjacent rotor teeth, and then a rotor cell can be obtained. The non-magnetic support part as shown in Fig. 15 are used to combine the rotor cells into a completed rotor.

The measured open-circuit phase back-EMF waveforms of two machines at the rated speed of 1500r/min are shown in Fig. 17. The phase back-EMF waveforms of two machines are satisfied agreement with the corresponding 3D-FEA results, respectively. From the Fourier analysis, the fundamental component of the measured phase back-EMF in the RPM-FS machine is 211V, being about 95% of the 3D-FEA result.

Meanwhile, the measured and FEA-predicted THD values are 9.97% and 11.65%, respectively. For the SPM-FS machine, the fundamental component of the measured back-EMF is 95% of that 3D-FEA result (256V). The THD values from the measurement and FEA prediction is 2.36% and 1.72%, respectively. The minor discrepancies between the measured and 3D-FEA results can be mainly attributed to the imperfection of manufacturing and assembling process.

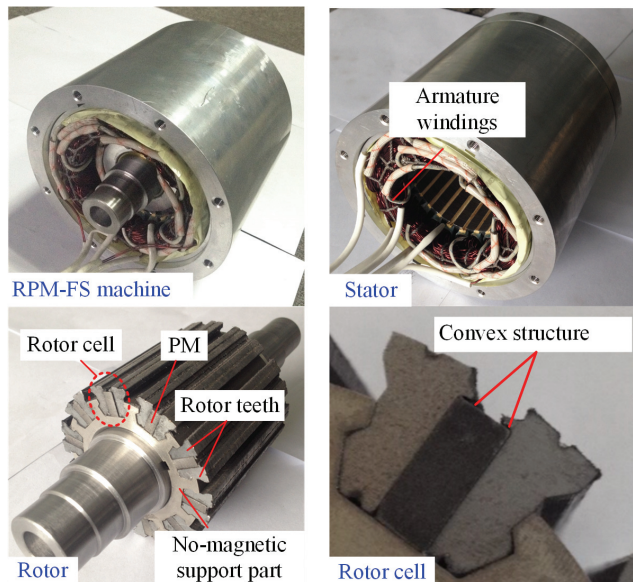


Fig. 15 The prototype of the RPM-FS machine.

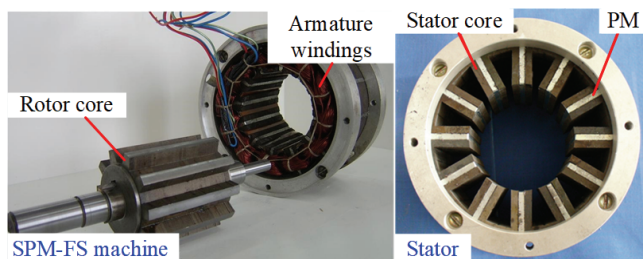


Fig. 16 The prototype of the SPM-FS machine.

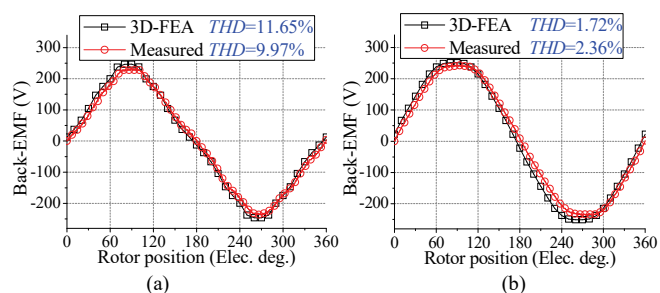


Fig. 17 Phase back-EMF waveforms at rated speed of 1500rpm. (a) RPM-FS machine. (b) SPM-FS machine.

The output torque and efficiency of two machines versus current density are shown in Fig. 18, where $i_d=0$ control is employed and the PM operating temperature is estimated to be 90°C for 3D-FEA, since the PM demagnetization caused by high temperature will contribute to the discrepancies. These torque values are measured at the speed of 1500r/min. As can be seen, the measured output torques of two machines increases linearly as armature current density rises, and the 3D-FEA

results agree well with measured results. It can be found from Fig. 18(a) that the measured output torque of the RPM-FS machine at rated current density is 15Nm, which is about 95% of the 3D-FEA prediction. However, for the SPM-FS machine, the measured rated torque is 11.8Nm, which is 91% of the 3D-FEA result at $J_{a,rms}=5A/mm^2$. The error can be attributed to the manufacturing tolerances and partial irreversible demagnetization in the PMs due to high temperature under over-load experiments. In addition, the measured efficiencies of both machines are lower than the 3D-FEA results, since the mechanical losses in two machine are estimated inaccurately and the output torque decreases as above analysis. At the rated operation point, the measured efficiencies of two machines are almost the same, being about 86.3% and 86.15%, respectively.

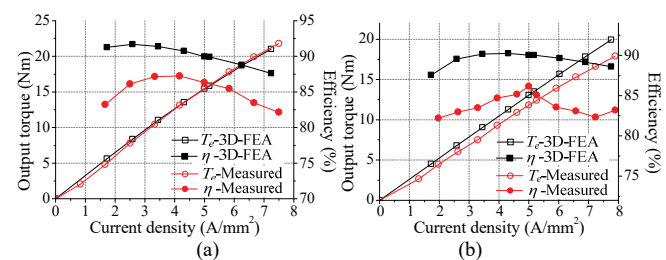


Fig. 18 Output torque and efficiency versus different current densities at the rated speed of 1500r/min. (a) RPM-FS machine. (b) SPM-FS machine.

V. CONCLUSIONS

In this paper, a comprehensive comparison between a 24s/10p RPM-FS machine and a 12s/10p SPM-FS machine is conducted with the same overall dimensions, main material properties, current density, and DC-link bus voltage. The electromagnetic torque performances of two flux-switching machines are analyzed and compared from two perspectives, i.e. magnetic field modulation and torque-sizing equation. Some conclusions can be summarized as followed.

1) The RPM-FS and SPM-FS machines are both featured with doubly-salient structures. Hence, both the primitive PM-MMF and armature reaction-MMF are modulated by the salient iron cores in air-gap field.

2) The electromagnetic torque of the RPM-FS machine is mainly contributed by the PM-MMF harmonics with rotor-PM pole-pair number (83%). However, for the SPM-FS machine, T_e is not only produced by the primitive PM-MMF harmonics with 6th and 18th, but also generated by the modulated PM-MMF harmonic components, i.e. 4th, 8th, 16th, and 28th.

3) For RPM-FS machines, the PMs are removed from stator to rotor, which results in a significant alleviation of the slot areas for armature windings. Hence, the electrical loading is improved effectively and the magnetization saturation of stator teeth can be reduced correspondingly. Consequently, the torque characteristics can be significantly improved.

4) The speed regulation range of the SPM-FS machine is unfavorably narrower than the RPM-FS machine, since the former exhibits a higher PM flux linkage and lower d -axis armature reaction flux-linkage L_{ad} . In addition, the flux-weakening capability of RPM-FS machine can be enhanced further by adjusting the k_{hrr} , meanwhile, the output torque sacrifices correspondingly.

5) The PM utilization ratio of the RPM-FS machine is considerably larger than the SPM-FS machine, which dramatically influences the material cost consumed.

6) The PMs of the RPM-FS machines are located in the rotor, and consequently, the rotor structure is more complex than the SPM-FS machines. Further, the mechanical strength investigation of RPM-FS machines especially under high-speed is the work undergoing.

In general, the torque production mechanism of flux switching machines with different topologies can be investigated based on filed modulation principle and magnetic gearing effect. On the other hand, the torque capability and speed regulation capacity are dominantly determined by the magnetic and electrical loadings, which should be improved by optimizing the key geometric dimensions or investigating novel topologies.

REFERENCES

- [1] E. Hoang, A. H. Ben-Ahmed, and J. Lucidarme, "Switching flux permanent magnet polyphased synchronous machines," in *Proc. Eur. Conf. Power Electron. Appl.*, 1997, pp. 903–908.
- [2] X. Zhu, D. Fan, L. Mo, Y. Chen, and L. Quan, "Multi-objective optimization design of double-rotor flux-switching permanent magnet machine considering multi-Mode operation" *IEEE Trans. Ind. Electron.*, vol. 66, no. 1, pp. 641-653, Jan. 2019.
- [3] D. J. Evans, and Z. Q. Zhu. "Novel partitioned stator switched flux permanent magnet machines." *IEEE Trans. Magn.*, vol. 51, no. 1, pp. 8100114, Jan. 2015.
- [4] P. Su, W. Hua, G. Zhang, Z. Chen, M. Cheng. "Analysis and evaluation of novel rotor permanent magnet flux-switching machine for EV and HEV applications." *IET Electr. Power App.*, DOI: 10.1049/iet-epa.2017.0182.
- [5] J. D. McFarland, T. M. Jahns, and A. M. EL-Refai. "Analysis of the torque production mechanism for flux-switching permanent-magnet machines." *IEEE Trans. on Ind. Appl.*, vol. 51, no. 4, pp. 3041-3049, Jul./Aug. 2015.
- [6] M. Cheng, P. Han, W. Hua. "A general airgap field modulation theory for electrical machines." *IEEE Trans. Ind. Electron.*, vol. 64, no. 8, pp. 6063-6074, March. 2017.
- [7] Z. Z. Wu, and Z. Q. Zhu, "Analysis of air gap field modulation and magnetic gearing effects in switched flux permanent magnet machines." *IEEE Trans. Magn.*, vol. 51, no. 5, pp. 8105012, May 2015.
- [8] X. Zhu, Z. Xiang, L. Quan, W. Wu, and Y. Du, "Multi-Mode optimization design methodology for a flux-controllable stator permanent magnet memory motor considering driving cycles," *IEEE Trans. Ind. Electron.*, vol. 65 no. 7, pp. 5353-5366, Jul. 2018.
- [9] D. Li, R. Qu, W. Xu, J. Li, T. A. Lipo, "Design procedure of dual-stator spoke-array vernier permanent-magnet machines," *IEEE Trans. Ind. Appl.*, vol. 54, no. 4, pp. 2972-2983, Jul./Aug. 2015.
- [10] A. Mahmoudi, S. Kahourzade, N.A. Rahim, and W.P. Hew, "Design, analysis, and prototyping of an axial-flux permanent magnet motor based on genetic algorithm and finite-element analysis," *IEEE Trans. Magn.*, vol. 49, no. 4, pp. 1479-1492, Apr. 2013.
- [11] W. Fei, P. Luk, J. X. Shen, Y. Wang and M. Jin, "A novel permanent-magnet flux switching machine with an outer-rotor configuration for in-wheel light traction applications," *IEEE Trans. Ind. Appl.*, vol. 48, no. 5, pp. 1496-1506, Sep./Oct. 2012.
- [12] G. Zhang, W. Hua, and M. Cheng. "Design and comparison of two six-phase hybrid-excited flux-switching machines for EV/HEV applications." *IEEE Trans. Ind. Electron.*, vol. 63, no. 1, pp. 481-493, Jan. 2016.
- [13] P. Su, W. Hua, Z.Z. Wu, P. Han, M. Cheng. "Analysis of the operation principle for rotor permanent magnet flux switching machines." *IEEE Trans. Ind. Electron.*, DOI: 10.1109/TIE.2017.2733442.
- [14] N. Bianchi, M. D. Pre, L. Alberti, E. Fornasiero. "Theory and design of fractional-slot PM machine." 1st ed. Padova, Italy: CLEUP, 2007.
- [15] G. Lei, C. Liu, J. Zhu and Y. Guo, "Techniques for Multilevel Design Optimization of Permanent Magnet Motors." *IEEE Trans. Energy Covers.*, vol. 30, no. 4, pp. 1574-1584, Dec. 2015.
- [16] X. Zhu, Z. Xiang, C. Zhang, L. Quan, Y. Du, and W. Gu, "Co-reduction of torque ripple for outer rotor flux-switching PM motor using systematic multi-level design and control schemes", *IEEE Trans. Ind. Electron.*, vol. 64, no. 2, pp. 1102-1112, Feb. 2017.
- [17] Yamazaki, K., "Torque and efficiency calculation of an interior permanent magnet motor considering harmonic iron losses of both the stator and rotor," *IEEE Trans. Magn.*, vol. 39, no. 3, pp. 1460-1463, May 2003.
- [18] Zhu, S., Cheng, M., Dong, J., Du, J., "Core loss analysis and calculation of stator permanent-magnet machine considering DC-biased magnetic induction," *IEEE Trans. Ind. Electron.*, vol. 61, no. 10, pp. 5203-5212, Oct. 2014.
- [19] X. Liu, H. Chen, J. Zhao and A. Belahcen, "Research on the performances and parameters of interior PMSM used for electric vehicles". *IEEE Trans. Ind. Electron.*, vol. 63, no. 6, pp. 3533-3545, Feb. 2016.



Peng Su (S'14) was born in Henan, China, in 1988. He received the B.Sc. and M.E. degrees in electrical engineering from Henan Polytechnic University, Henan, China in 2011 and 2013, respectively. Since 2013, he has been with the School of Electrical Engineering, Southeast University, Nanjing, China, where he is currently working toward the Ph.D. degree. From December 2016 to December 2017, he was a joint Ph.D. student funded by China Scholarship Council in the Department of Energy Technology, Aalborg University, Aalborg, Denmark.

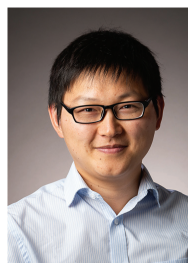
His current research interests include the design and analysis of novel permanent-magnet brushless electrical machines for application in electric vehicles.



Wei Hua (SM'16) was born in Taizhou, China, in 1978. He received the B.Sc. and Ph.D. degrees in electrical engineering from Southeast University, Nanjing, China, in 2001 and 2007, respectively.

Since 2007, he has been with Southeast University, where he is currently a Professor with the School of Electrical Engineering. He is the author or coauthor of more than 100 technical papers and is the holder of 44 patents in his areas of interest. His teaching and

research interests include the design, analysis, and control of electrical machines.



Zhongze Wu (S'15-M'18) received the B.Eng. and M.Sc. degrees in electrical engineering from the Chien-Shiung Wu College and the School of Electrical Engineering, Southeast University, Nanjing, China, in June 2010 and March 2013, respectively, and the Ph.D. degree in Electronic and Electrical Engineering from The University of Sheffield, Sheffield, U.K., in January 2017.

Since August 2018, he has been with Powertrain and Vehicle Research Centre, Department of Mechanical Engineering, University of Bath, Bath, U.K., where he is currently a Prize Fellow. His current research interests include the analysis, design, control and manufacturing of advanced machines and drives for electric propulsion systems.

From January 2017 to August 2018, he was with Warwick Manufacturing Group (WGM), University of Warwick, Coventry, U.K., as a research fellow.



Zhe Chen (M'95–SM'98) received the B.Eng. and M.Sc. degrees all in electrical engineering from Northeast China Institute of Electric Power Engineering, Jilin City, China, in 1982 and 1986, respectively, the M.Phil. degree in power electronic from Staffordshire University, Staffordshire, U.K., in 1993, and the Ph.D. degree in power and control from University of Durham, Durham, U.K., in 1997.

He is a Full Professor with the Department of Energy Technology, Aalborg University, Aalborg, Denmark, since 2002. He is the Danish Principle Investigator for Wind Energy of Sino-Danish Centre for Education and Research and the leader of Wind Power System Research program at the Department of Energy Technology, Aalborg University. He has led many international and national research projects and has more than 500 technical publications with more than 12500 citations (Google Scholar) and h-index of 49. His research interests include power systems, power electronics, and electric machines; and his main current research interests are wind energy and modern power systems.

Dr. Chen is an Associate Editor of the IEEE TRANSACTIONS ON POWER ELECTRONICS, a Fellow of the Institution of Engineering and Technology, London, U.K., and a Chartered Engineer in the U.K.



Gan Zhang (M'15) was born in Shandong Province, China. He received the B.Sc. and Ph.D. degrees in electrical engineering from the School of Electrical Engineering, Southeast University, Nanjing, China, in 2011 and 2016, respectively. From January 2015 to February 2016, he was a joint Ph.D. student funded in the Department of Energy Technology, Aalborg University, Aalborg, Denmark.

Since 2016, he has been with Southeast University, where he is currently a Lecturer with the School of Electrical Engineering. His teaching and research interests include the design and analysis of novel permanent-magnet brushless electrical machines, and electric vehicle technology.



Ming Cheng (M'01–SM'02–F'15) received the B.Sc. and M.Sc. degrees in Electrical Engineering from the Department of Electrical Engineering, Southeast University, Nanjing, China, in 1982 and 1987, respectively, and the Ph.D. degree from the Department of Electrical and Electronic Engineering, The University of Hong Kong, Hong Kong, in 2001.

Since 1987, he has been with Southeast University, where he is currently a Distinguished Professor in the School of Electrical Engineering and the Director of the Research Center for Wind Power Generation. From January to April 2011, he was a Visiting Professor with the Wisconsin Electric Machine and Power Electronics Consortium, University of Wisconsin-Madison. His teaching and research interests include electrical machines, motor drives for electric vehicles, and renewable energy generation. He has authored or coauthored over 350 technical papers and 4 books and is the holder of 90 patents in these areas.

Prof. Cheng is a fellow of the Institution of Engineering and Technology. He has served as chair and organizing committee member for many international conferences. He is a Distinguished Lecturer of the IEEE Industry Applications Society (IAS) in 2015/2016.